JACS
JOURNAL OF THE AMERICAN CHEMICAL SOCIETY

Communication

pubs.acs.org/JACS

Thickness-Controlled Quasi-Two-Dimensional Colloidal PbSe Nanoplatelets

Weon-kyu Koh,[†,⊥] Naveen K. Dandu,[‡,⊥] Andrew F. Fidler,[†] Victor I. Klimov,[†] Jeffrey M. Pietryga,*[,†] and Svetlana V. Kilina*[,‡]

[†]Center for Advanced Solar Photophysics, C-PCS, Chemistry Division, Los Alamos National Laboratory, Los Alamos, New Mexico 87545, United States

[‡]Department of Chemistry and Biochemistry, North Dakota State University, Fargo, North Dakota 58108, United States

Supporting Information

ABSTRACT: We demonstrate controlled synthesis of discrete two-dimensional (2D) PbSe nanoplatelets (NPLs), with measurable photoluminescence, via oriented attachment directed by quantum dot (QD) surface chemistry. Halide passivation is critical to the growth of these (100) face-dominated NPLs, as corroborated by density functional theory studies. $PbCl_2$ moieties attached to the (111) and (110) of small nanocrystals form interparticle bridges, aligning the QDs and leading to attachment. We find that a 2D bridging network is energetically favored over a 3D network, driving the formation of NPLs. Although PbI_2 does not support bridging, its presence destabilizes the large (100) faces of NPLs, providing means for tuning NPL thickness. Spectroscopic analysis confirms the predicted role of thickness-dependent quantum confinement on the NPL band gap.

Shape control offers unique means for manipulation of semiconductor nanocrystals' electronic properties, including dynamical behavior. For example, because the band gap of quasi-one-dimensional (1D) nanorods[1] can be tuned by restricting particle size in only two dimensions, elongation in the third dimension can be used to alter charge carrier recombination and cooling processes, substantially impacting the efficiencies of Auger recombination and "carrier multiplication" (CM),[2] as well as optical gain properties.[3] Such effects are potentially even greater in quasi-two-dimensional (2D) nanostructures such as nanoribbons[4] and nanoplatelets (NPLs).[5] Indeed, 2D colloidal II-VI NPLs have recently been shown to offer efficient, very narrow emission[6] that is tunable as a function of thickness,[5a] as well as unique carrier cooling dynamics,[7] reduced Auger recombination rates[8] and low amplified spontaneous emission thresholds.[8b,9]

2D nanostructures of PbSe are attractive for use in solar cells and infrared light-emitting diodes and lasers. Although most QD-based solar cells to date have used PbS QDs,[10] PbSe QDs exhibit higher CM efficiencies,[2c,11] enabling solar cells with quantum efficiencies greater than unity.[12] PbSe NPLs may exhibit further enhanced CM and device efficiencies, while properly aligned NPL films can potentially offer improved charge transport. Additionally, reduced Auger recombination rates and high absorption cross sections may allow low-threshold lasing at infrared wavelengths of importance to telecommunications[13] and remote sensing.[14]

Although PbSe NPLs of discrete lateral dimensions are yet unknown, examples of nanosheet formation suggest a path forward. Schliehe et al. found that chloroalkanes, as "lead complexing agents", slowed growth and triggered 2D oriented attachment of PbS QDs, driven by the reactivity of (110) faces that remain present in small QDs.[15] However, we suggest that later studies indicate that Cl-containing species may play a more active role than merely slowing reaction. In a synthesis of PbSe nanosheets without chlorine-containing species,[16] (110)-oriented attachment was instead promoted by the presence of excess lead acetate, which was said to "block" further reaction at (100) faces. At the same time, the ability of chlorine to enhance the stability of PbS and PbSe QDs against oxidation[17] has been attributed to surface reactions specifically with (100) faces.[18] Finally, facet-specific binding of Cl^- has been shown to have a profound effect on the shape of cadmium chalcogenide nanocrystals.[19]

Accordingly, to synthesize 2D PbSe NPLs, we focused on determining the role of halides in oriented attachment. We find that excess Cl^- or Br^- during synthesis of PbSe QDs indeed results in formation of NPLs of constant thickness and limited lateral size. Intriguingly, although the use of I^- precursors alone does not lead to NPL growth, the presence of I^- in mixed halide reactions allows the formation of thicker NPLs. Density functional theory (DFT) calculations help elucidate the complex roles halides play in NPL formation. They reveal that Cl^--rich conditions promote 2D oriented attachment by instigating the formation of inter-QD bridges. On the other hand, I^- does not support bridge formation, but reactivates the large (100) faces of NPLs toward attachment in a manner not seen previously in nanosheets, allowing stepwise thickening. Finally, we apply absorption and PL spectroscopy to verify that thickness is the dominant contributor to confinement energy for these NPLs.

In a typical synthesis of PbSe NPLs, $PbCl_2$ and Se powder react in a mixture of alkyl amines and quaternary ammonium chlorides, and the products are collected by precipitation and redispersed in chloroform (see Supporting Information for details). Some turbidity is often observed in the dispersion,

Received: November 18, 2016
Published: January 18, 2017

DOI: 10.1021/jacs.6b11945
J. Am. Chem. Soc. 2017, 139, 2152–2155

suggesting aggregation; addition of a small amount of oleic acid prior to precipitation enhances product solubility.

Transmission electron microscopy (TEM, Figure 1a) reveals rectangular PbSe NPLs; the lattice spacing and elemental

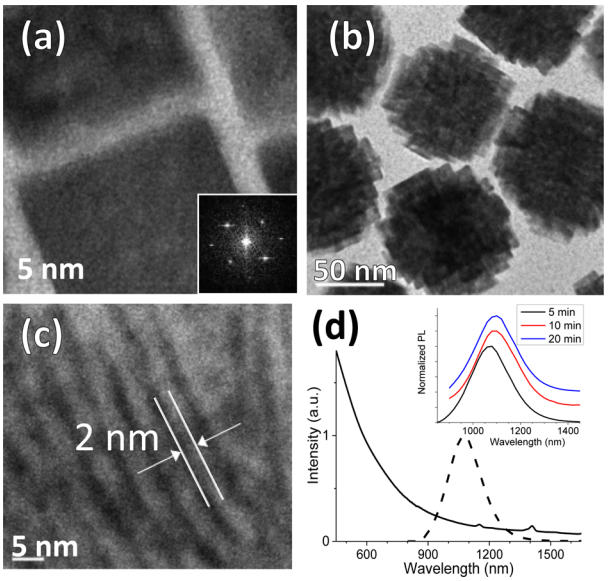

Figure 1. (a) TEM image of PbSe NPL synthesized using $PbCl_2$. Inset: electron diffraction verifyies the rock-salt crystal structure. (b) Top-down and (c) side-on TEM images of face-to-face stacks of NPLs. (d) Absorption (solid) and PL (dashed) spectra of NPLs. Inset: The PL peak redshifts slightly as QDs attach to form NPLs, then remains constant.

analysis (Table S1) confirm that the large faces are the (100) plane of rock-salt PbSe. Images from early reaction aliquots show small PbSe QDs form first, and then fuse via oriented attachment to create PbSe NPLs (Figure S1). TEM images also show that NPL aggregation (when oleic acid is not added during purification) occurs via face-to-face stacking (Figure 1b); side-on views of stacks reveal that regardless of reaction time or temperature, the NPLs are consistently ~2 nm thick (Figure 1c). Absorption spectra of NPLs do not show a discernible band-edge feature, but a weak PL feature (~0.1% quantum yield) is typically found at 1100 nm (Figure 1d).

Seeking insights into NPL formation, we modeled QDs of ~1 nm ($Pb_{16}Se_{16}$) and ~2 nm ($Pb_{68}Se_{68}$) diameter, built up from a bulk rock-salt lattice as described elsewhere.[20] Both QDs exhibit three main surfaces: (100), (110) and (111) (Figure 2a). We used DFT to study the surface-specific binding of various species from the reaction mixture (Figure 2b, with NH_2Me as a representative primary amine), including geometry optimization of QDs after ligation (Figure S6), using propylamine as solvent. Calculations of the QD–ligand binding energies reveal varying degrees of face selectivity. In particular, Pb^{2+} cations strongly and preferentially bind to the (110) and selenium-rich (111) surfaces of the $Pb_{68}Se_{68}$ QD (Figure 2b), whereas amines are the weakest interacting species, and preferentially bind to the stoichiometric (100) surface. Under growth conditions, we would expect many ligands to bind to a given QD; hence, in Figure 2c we show the binding energy of each subsequent ligand as the total number of ligands increases. Unlike other species, the interaction strength of bare Pb^{2+} decreases dramatically as the number of attached ions increases. Considering the Cl^--rich environment, this suggests that (110)

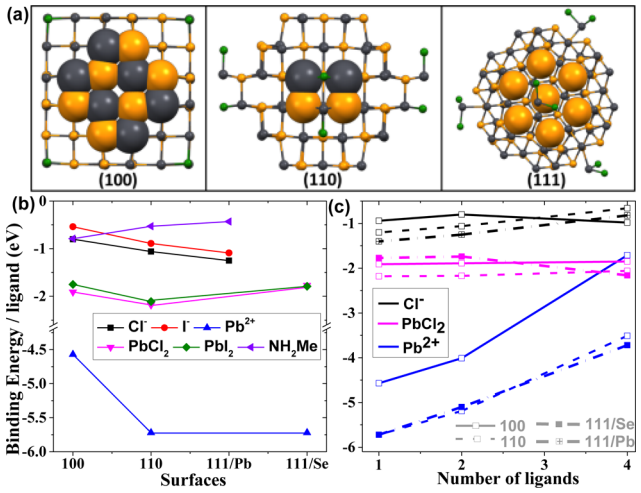

Figure 2. (a) Main crystallographic surfaces of $Pb_{68}Se_{68}$: six (100), twelve (110), and four Pb-terminated and four Se-terminated (111). Yellow = Se; gray = Pb; green = Cl. This model shows one $PbCl_2$ attached to each (110) face. (b) Surface-specific ligand binding energies calculated in propylamine solvent medium. (c) Scaling of the energies in (b) with increasing QD ligand coverage of the entire QD. I^--containing species (omitted) follow the trends of their Cl^--containing equivalents.

and (111) faces are ligated heavily by $PbCl_2$, either from direct binding from solution, or through Cl^- binding to already surface-bound Pb^{2+} ions. Similar trends are observed for smaller $Pb_{16}Se_{16}$ QD (see Supporting Information for all computational details).

$PbCl_2$ units attached to (111) and (110) faces are key to NPL formation, as they adopt "bridging" positions between small QDs (Figure S7). For more realistic analysis of QD–QD interactions, we utilize periodic boundary conditions to mimic 2D and 3D QD attachment. Starting with the optimized $Pb_{68}Se_{68}$ with (110) surfaces fully or partially passivated by $PbCl_2$, the final 2D structures of NPLs exhibit a Pb–Cl–Pb bridging network that rigidly aligns neighboring QDs along the (100) lattice direction (Figure 3a, Table S4). Importantly, the calculated Pb–Cl bond length is very similar to that of Pb–Se, so in effect, Cl^- ions adopt the selenium positions of an extrapolated lattice, which facilitates fusion and subsequent ingrowth to form a continuous NPL (Figure 3b).

Our calculations of surface energy (Figure 3d, and Table S5) also show that 2D networking (ultimately leading to NPLs) is energetically favored over 3D attachment. Moreover, addition of amines to the (100) surfaces that are not involved in the 2D network (i.e., the top and bottom of a NPL) dramatically reduces the surface energy even further, essentially locking out growth in this direction. Finally, we find that the surface energy of 2D structures formed by $Pb_{16}Se_{16}$ (thickness ~1 nm) are significantly less stable compared to those made of $Pb_{68}Se_{68}$ QDs (~2 nm), suggesting that continued growth, rather than attachment, is favored for smaller QDs. This agrees with the experimentally observed NPL thickness of ~2 nm.

These calculations suggest that a combination of $PbCl_2$, excess Cl^- and amines is critical to NPL formation. For comparison, the same model QDs passivated with PbI_2/I^- do not form bridges, despite interaction strengths very similar to those of $PbCl_2$ (Figure 2b,c), due to the mismatch between Pb–I and Pb–Se bond lengths (Figure 3c). These findings match experiment: use of either $PbCl_2$ or $PbBr_2$ (Figure S2; not

DOI: 10.1021/jacs.6b11945
J. Am. Chem. Soc. 2017, 139, 2152–2155

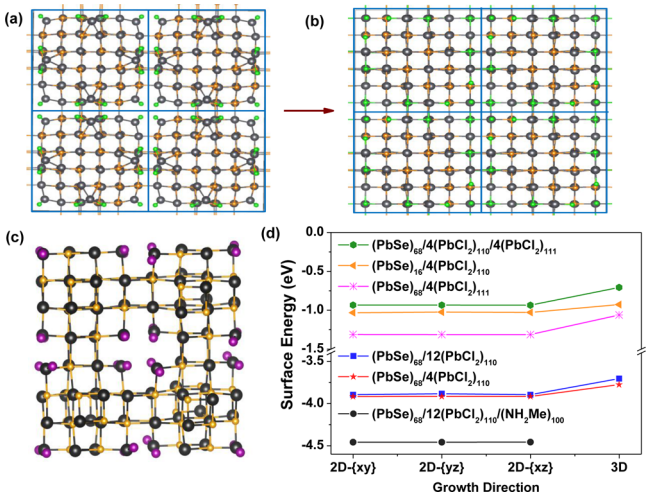

Figure 3. Geometries of $Pb_{68}Se_{68}$ with fully $PbCl_2$-passivated (110) surface (a) before and (b) after optimization. The 2D network is stabilized by Pb−Cl−Pb bridges connecting neighboring QDs along (100) surfaces. (c) Optimized geometry of a 2D structure constructed from $Pb_{16}Se_{16}$ with PbI_2-passivated (110) surfaces. Lack of Pb−I−Pb bridging reduces ordering and destabilizes the 2D array. (d) Calculated surface energies as a function of 2D and 3D superlattice growth direction constructed from $Pb_{16}Se_{16}$ or $Pb_{68}Se_{68}$ QDs with $PbCl_2$ ligands passivating (110), (111) or both surfaces. Black trace shows stabilizing effect of NH_2Me passivation of (100) facets (which precludes 3D networking).

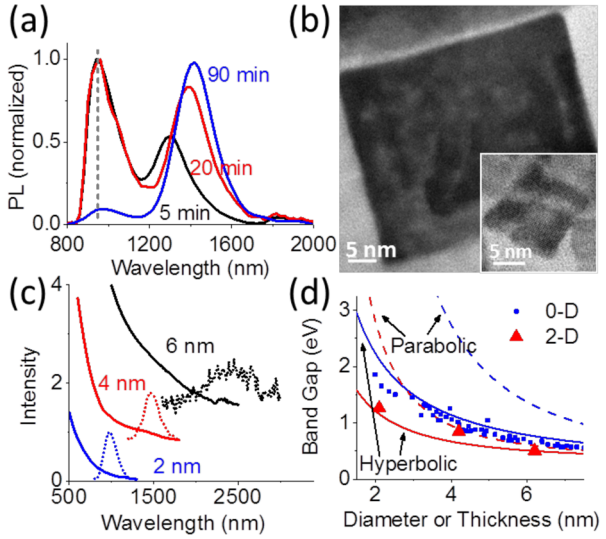

Figure 4. (a) Evolution of PL of NPLs during PbI_2 reaction. (b) Main panel and inset show TEM images of NPLs during the transition between 2 and 4 nm thickness. (c) Absorption (solid) and PL spectra of samples dominated by NPLs of distinct thicknesses. PL quantum yields for 4 nm samples are typically 0.04%; those of thicker samples are at least an order of magnitude lower. (d) Parabolic (dash) and hyperbolic (solid) band model of PbSe 0D QDs (blue) and 2D NPLs (red). Symbols denote SAXS thicknesses (NPLs, Figure S5) or literature diameters (QDs[24]).

modeled) results in NPLs, while the small QDs initially formed in PbI_2 reactions randomly aggregate but do not form distinct and regularly shaped NPLs (Figure S3). Regardless of lead precursor, NPLs are not produced without an additional source of halide ion. A number of alkylammonium chloride precursors can be used to produce NPLs using $PbCl_2$, and either Cl^- or Br^- sources (such as tetrabutylammonium bromide) are effective in $PbBr_2$ reactions. In all cases, the PL peak energy remains the same, confirming that NPLs form by attachment of QDs of a critical size (2 nm; Figure S1).

Spectra taken during reactions using PbI_2 with excess Cl^- reveal more complex behavior: soon after it emerges, the PL peak begins to diminish in intensity, while a second peak at ∼1300−1400 nm begins to grow (Figure 4a). TEM images of samples during this transition reveal NPLs that are mottled in appearance, suggesting thickening of NPLs via attachment to the large faces (Figure 4b). After 90 min of reaction, the redder PL peak is dominant, and the majority of NPLs have become more-or-less evenly ∼4 nm in thickness. At still longer times (3 h), the PL peak again fades as a very weak feature at 2400 nm emerges (Figure 4c). At this point, TEM reveals ∼6.5 nm thick NPLs (Figure S4). Further heating yields insoluble products without measurable emission.

Compared to reports of PbS and PbSe nanosheets,[15,16] attachment-based thickness control of this manner is unique. The formation of 2 nm thick NPLs from reactions with PbI_2 and excess Cl^- ions shows that Pb−Cl−Pb bridging still occurs. This can result from the in situ formation of $PbCl_2$, driven by the greater Pb−Cl bond strength (2.5 eV, vs 1.5 eV for Pb−I),[21] or from PbI_2 binding to the reactive (110) and (111) QD surfaces, followed by exchange of the I^- for Cl^- ions. NPL thickening, however, requires that the amine-passivated (100) faces become chemically active. DFT calculations show that either PbX_2 precursor (X = Cl or I) can displace an amine ligand and bind to the (100) surface of $Pb_{68}Se_{68}$. Once there, it dissociates into PbX^+ and X^-, attaching to surface Se and Pb sites, respectively (Figure S9). In the case of Cl^-, the displaced amine binds to the $PbCl^+$ moiety and continues to block the (100) surface as before. However, in the I^- case, the PbI^+ fragment migrates to the adjacent Se-rich (111) surface, allowing the amine to leave the surface, creating an opening in the passivation of the (100) face for attachment of either another NPL fragment or 2 nm QD. Thus, the incremental thickening of NPLs over prolonged reaction time results from PbI_2's ability to "clean" the (100) faces of amines.

The ability to synthesize NPLs of three distinct thicknesses, all with measurable emission, allows us to probe the effects of quantum confinement in 2D PbSe system for the first time. The thickness-dependent PL energies for NPLs in this study are shown in Figure 4d (red triangles). For estimating confinement energy, the effective mass approximation typically fails for PbSe QDs (blue dashed line) due to the highly nonparabolic curvature of the conduction and valence bands near the L point.[22] Alternatively, we apply a hyperbolic band model that has proven useful for modeling of Pb chalcogenide QDs (blue solid line).[23] This model shows reasonable agreement with NPL data, supporting that the thickness of NPLs is the dominant contribution to their confinement energy. We note that the previously reported PbS nanosheet with 2.2 nm thick and ∼800 nm emission peak[15] is also consistent with our hyperbolic model.

In conclusion, we synthesized the first quasi-2D PbSe NPLs using oriented attachment, with thickness controlled by choice of lead halide precursor. DFT calculations show that $PbCl_2$ strongly interacts with the (110) and (111) sites of small PbSe QDs, instigating Pb−Cl−Pb bridging with neighboring QDs along the (100) lattice direction which ultimately leads to NPLs. Although PbI_2 is incapable of such bridging, the presence of PbI_2 mixed with excess Cl^- activates NPL faces toward

DOI: 10.1021/jacs.6b11945
J. Am. Chem. Soc. 2017, 139, 2152−2155

attachment of QDs or NPL fragments, resulting in NPLs of larger thicknesses. Finally, we find that the effective mass approximation with a hyperbolic band model reasonably explains the observed thickness dependence of the bandgap, as determined by PL measurements.

■ ASSOCIATED CONTENT

Supporting Information

The Supporting Information is available free of charge on the ACS Publications website at DOI: 10.1021/jacs.6b11945.

Detailed descriptions of synthesis, characterization, DFT methods, band gap calculations, and additional TEM images (PDF)

■ AUTHOR INFORMATION

Corresponding Authors

*pietryga@lanl.gov

*svetlana.kilina@ndsu.edu

ORCID

Victor I. Klimov: 0000-0003-1158-3179

Jeffrey M. Pietryga: 0000-0001-5360-4228

Svetlana V. Kilina: 0000-0003-1350-2790

Author Contributions

⊥These authors contributed equally.

Notes

The authors declare no competing financial interest.

■ ACKNOWLEDGMENTS

W.-k.K. and J.M.P. were supported by the Los Alamos National Laboratory (LANL) LDRD program. A.F.F. and V.I.K were supported by the Center for Advanced Solar Photophysics (CASP), an Energy Frontier Research Center funded by the U.S. Department of Energy (DOE), Office of Science, Office of Basic Energy Sciences. N.D. and S.K. acknowledge the U.S. DOE (DE-SC008446) for financial support, and NERSC (DE-AC02-05CH11231) and the Center for Integrated Nanotechnology (LANL) for computational resources and facilities; a Sloan Research Fellowship BR2014-073 supported software license purchase. The authors thank Darrick J. Williams for SAXS analysis.

■ REFERENCES

(1) (a) Manna, L.; Scher, E. C.; Alivisatos, A. P. *J. Am. Chem. Soc.* **2000**, *122*, 12700. (b) Talapin, D. V.; Nelson, J. H.; Shevchenko, E. V.; Aloni, S.; Sadtler, B.; Alivisatos, A. P. *Nano Lett.* **2007**, *7*, 2951. (c) Koh, W.-k.; Bartnik, A. C.; Wise, F. W.; Murray, C. B. *J. Am. Chem. Soc.* **2010**, *132*, 3909.

(2) (a) Htoon, H.; Hollingsworth, J.; Dickerson, R.; Klimov, V. *Phys. Rev. Lett.* **2003**, *91*, 227401. (b) Padilha, L. A.; Stewart, J. T.; Sandberg, R. L.; Bae, W. K.; Koh, W. K.; Pietryga, J. M.; Klimov, V. I. *Nano Lett.* **2013**, *13*, 1092. (c) Padilha, L. A.; Stewart, J. T.; Sandberg, R. L.; Bae, W. K.; Koh, W. K.; Pietryga, J. M.; Klimov, V. I. *Acc. Chem. Res.* **2013**, *46*, 1261.

(3) (a) Gao, S.; Zhang, C.; Liu, Y.; Su, H.; Wei, L.; Huang, T.; Dellas, N.; Shang, S.; Mohney, S. E.; Wang, J.; Xu, J. *Opt. Express* **2011**, *19*, 5528. (b) Moreels, I.; Rainò, G.; Gomes, R.; Hens, Z.; Stöferle, T.; Mahrt, R. F. *Adv. Mater.* **2012**, *24*, OP231. (c) Htoon, H.; Hollingworth, J. A.; Malko, A. V.; Dickerson, R.; Klimov, V. I. *Appl. Phys. Lett.* **2003**, *82*, 4776.

(4) (a) Joo, J.; Son, J. S.; Kwon, S. G.; Yu, J. H.; Hyeon, T. *J. Am. Chem. Soc.* **2006**, *128*, 5632. (b) Liu, Y.-H.; Wang, F.; Wang, Y.; Gibbons, P. C.; Buhro, W. E. *J. Am. Chem. Soc.* **2011**, *133*, 17005.

(5) (a) Ithurria, S.; Dubertret, B. *J. Am. Chem. Soc.* **2008**, *130*, 16504. (b) Ithurria, S.; Tessier, M. D.; Mahler, B.; Lobo, R. P. S. M.; Dubertret, B.; Efros, A. L. *Nat. Mater.* **2011**, *10*, 936. (c) Li, Z.; Peng, X. *J. Am. Chem. Soc.* **2011**, *133*, 6578.

(6) Tessier, M. D.; Mahler, B.; Nadal, B.; Heuclin, H.; Pedetti, S.; Dubertret, B. *Nano Lett.* **2013**, *13*, 3321.

(7) (a) Pelton, M.; Ithurria, S.; Schaller, R. D.; Dolzhnikov, D. S.; Talapin, D. V. *Nano Lett.* **2012**, *12*, 6158. (b) Achtstein, A. W.; Schliwa, A.; Prudnikau, A.; Hardzei, M.; Artemyev, M. V.; Thomsen, C.; Woggon, U. *Nano Lett.* **2012**, *12*, 3151.

(8) (a) Kunneman, L. T.; Tessier, M. D.; Heuclin, H.; Dubertret, B.; Aulin, Y. V.; Grozema, F. C.; Schins, J. M.; Siebbeles, L. D. A. *J. Phys. Chem. Lett.* **2013**, *4*, 3574. (b) She, C.; Fedin, I.; Dolzhnikov, D. S.; Demortière, A.; Schaller, R. D.; Pelton, M.; Talapin, D. V. *Nano Lett.* **2014**, *14*, 2772.

(9) (a) Guzelturk, B.; Kelestemur, Y.; Olutas, M.; Delikanli, S.; Demir, H. V. *ACS Nano* **2014**, *8*, 6599. (b) She, C.; Fedin, I.; Dolzhnikov, D. S.; Dahlberg, P. D.; Engel, G. S.; Schaller, R. D.; Talapin, D. V. *ACS Nano* **2015**, *9*, 9475.

(10) (a) Luther, J. M.; Gao, J.; Lloyd, M. T.; Semonin, O. E.; Beard, M. C.; Nozik, A. J. *Adv. Mater.* **2010**, *22*, 3704. (b) Lan, X.; Voznyy, O.; García de Arquer, F. P.; Liu, M.; Xu, J.; Proppe, A. H.; Walters, G.; Fan, F.; Tan, H.; Liu, M.; Yang, Z.; Hoogland, S.; Sargent, E. H. *Nano Lett.* **2016**, *16*, 4630.

(11) Stewart, J. T.; Padilha, L. A.; Bae, W. K.; Koh, W.-K.; Pietryga, J. M.; Klimov, V. I. *J. Phys. Chem. Lett.* **2013**, *4*, 2061.

(12) Semonin, O. E.; Luther, J. M.; Choi, S.; Chen, H. Y.; Gao, J. B.; Nozik, A. J.; Beard, M. C. *Science* **2011**, *334*, 1530.

(13) Bakueva, L.; Musikhin, S.; Hines, M. A.; Chang, T.-W. F.; Tzolov, M.; Scholes, G. D.; Sargent, E. H. *Appl. Phys. Lett.* **2003**, *82*, 2895.

(14) (a) Rao, G. N.; Karpf, A. *Appl. Opt.* **2011**, *50*, A100.

(15) Schliehe, C.; Juarez, B. H.; Pelletier, M.; Jander, S.; Greshnykh, D.; Nagel, M.; Meyer, A.; Foerster, S.; Kornowski, A.; Klinke, C.; Weller, H. *Science* **2010**, *329*, 550.

(16) Lee, S.; Lee, D. T.; Ko, J.-H.; Kim, W.-J.; Joo, J.; Jeong, S.; McGuire, J. A.; Kim, Y.-H.; Lee, D. C. *RSC Adv.* **2014**, *4*, 9842.

(17) Bae, W. K.; Joo, J.; Padilha, L. A.; Won, J.; Lee, D. C.; Lin, Q.; Koh, W.-k.; Luo, H.; Klimov, V. I.; Pietryga, J. M. *J. Am. Chem. Soc.* **2012**, *134*, 20160.

(18) Woo, J. Y.; Ko, J.-H.; Song, J. H.; Kim, K.; Choi, H.; Kim, Y.-H.; Lee, D. C.; Jeong, S. *J. Am. Chem. Soc.* **2014**, *136*, 8883.

(19) (a) Kim, M. R.; Miszta, K.; Povia, M.; Brescia, R.; Christodoulou, S.; Prato, M.; Marras, S.; Manna, L. *ACS Nano* **2012**, *6*, 11088. (b) Meyns, M.; Iacono, F.; Palencia, C.; Geweke, J.; Coderch, M. D.; Fittschen, U. E. A.; Gallego, J. M.; Otero, R.; Juárez, B. H.; Klinke, C. *Chem. Mater.* **2014**, *26*, 1813.

(20) (a) Kamisaka, H.; Kilina, S. V.; Yamashita, K.; Prezhdo, O. V. *Nano Lett.* **2006**, *6*, 2295. (b) Kilina, S. V.; Craig, C. F.; Kilin, D. S.; Prezhdo, O. V. *J. Phys. Chem. C* **2007**, *111*, 4871. (c) Isborn, C. M.; Kilina, S. V.; Li, X.; Prezhdo, O. V. *J. Phys. Chem. C* **2008**, *112*, 18291. (d) Kamisaka, H.; Kilina, S. V.; Yamashita, K.; Prezhdo, O. V. *J. Phys. Chem. C* **2008**, *112*, 7800. (e) Kilina, S. V.; Kilin, D. S.; Prezhdo, V. V.; Prezhdo, O. V. *J. Phys. Chem. C* **2011**, *115*, 21641. (f) Hedrick, M. M.; Mayo, M. L.; Badaeva, E.; Kilina, S. *J. Phys. Chem. C* **2013**, *117*, 18216.

(21) Huheey, J. E. *Inorganic Chemistry: Principles of Structures and Reactivity*; Harper & Row: New York, 1972.

(22) Wang, Y.; Suna, A.; Mahler, W.; Kasowski, R. *J. Chem. Phys.* **1987**, *87*, 7315.

(23) Kang, I.; Wise, F. W. *J. Opt. Soc. Am. B* **1997**, *14*, 1632.

(24) (a) Koole, R.; Allan, G.; Delerue, C.; Meijerink, A.; Vanmaekelbergh, D.; Houtepen, A. J. *Small* **2008**, *4*, 127. (b) Sashchiuk, A.; Langof, L.; Chaim, R.; Lifshitz, E. *J. Cryst. Growth* **2002**, *240*, 431. (c) Yu, W. W.; Falkner, J. C.; Shih, B. S.; Colvin, V. L. *Chem. Mater.* **2004**, *16*, 3318.

DOI: 10.1021/jacs.6b11945
J. Am. Chem. Soc. 2017, 139, 2152−2155